Proceedings of the 21st ICSMGE, Vienna, Austria, 14 – 19 June 2026. Pistrol, Adam & Schweiger (eds.)
Published by: ÖGG, Austrian Society for Geomechanics, Salzburg, Austria, ISBN 978-3-9503898-4-5
https://doi.org/10.53243/ICSMGE2026-1082

Centrifuge modeling of suction anchor under out-of-plane loading in soft clay

Han Wu, Kunyu Li, Ying Lai*, Bin Zhu, Yunmin Chen
College of Civil Engineering and Architecture, Zhejiang University, Hangzhou, China, laiying@zju.edu.cn

ABSTRACT: This study explores how varying the out-of-plane (OOP) load angle Φ influences the bearing capacity and failure mechanisms of suction anchors. Using centrifuge model tests conducted at 50g, the research examined anchors positioned at their optimal embedment depth ($2L/3$) with a horizontal inclination of 35°. These tests were complemented by a limit equilibrium analysis to further understand the observed behaviors. When the out-of-plane load angle reached 30°, both the bearing performance and the ultimate bearing capacity experienced reductions of approximately 12%. As the angle decreased further below 30°, the failure mode shifted from sliding to a backward rotational failure, accompanied by gradual anchor torsion during loading. Based on the centrifuge test results and the limit equilibrium analysis, a weakening coefficient of 0.636 for the vertical component of soil shear strength due to torsion was determined. At a 90° out-of-plane load angle, the anchor experienced a substantial drop in performance, with bearing capacity and ultimate bearing capacity decreasing by roughly 60% and 19%, respectively, compared to in-plane loading conditions. For angles between 30° and 90°, the failure mode transitioned dramatically from sliding to a combined torsional and backward rotational failure. The failure process for anchors subjected to out-of-plane loads between 30° and 90° exhibited two distinct phases. Initially, as the external load increased, the anchor underwent significant torsion. Notably, the bearing capacity increased considerably with displacement during this stage. In the second phase, as the anchor's out-of-plane load angle reduced, the rate of torsion diminished. A relatively strong response was observed from soil pressure cells, indicating a continued rise in the anchor's bearing capacity.

KEYWORDS: Suction anchor, out-of-plane loading, centrifuge test, plastic limit analyses, capacity.

1 INTRODUCTION

Structurally, suction anchor foundations currently exhibit larger diameters and length-to-diameter ratios compared to other offshore mooring foundations, enabling them to provide relatively higher lateral and axial bearing capacities. Compared to other offshore anchoring foundations, suction anchor foundations offer advantages including simple design, ease of installation, and shorter installation periods (Aubeny, 2017).

In previous studies, researchers have predominantly concentrated on experimental, numerical, and theoretical investigations of in-plane monotonic or cyclic loading (Yan et al. 2024; Liu et al. 2024; Wu et al. 2024), with a scarcity of research addressing the torsional issues arising from out-of-plane angles (Φ). But in practical engineering applications, there were indeed scenarios where suction anchor foundations were subjected to out-of-plane loads. Although the impact of small out-of-plane angles (5°~10°) on the bearing capacity of suction anchors was accounted for during capacity estimation (Aubeny, 2017), however, investigations indicated that under strong environmental loading (e.g., high wave heights), the anchor chain experienced significant displacement, resulting in an estimated out-of-plane load on the suction anchor at an angle of approximately 30° (Colliat et al. 2018). Under extreme environmental loading, the failure of some mooring chains will cause the remaining mooring foundations to bear out-of-plane loads at angles exceeding 90°.

Ward et al. (2008) analyzed mooring system failures during Hurricanes Ivan, Katrina, and Rita, indicating that out-of-plane loading could cause the suction anchor to be pulled out and dragged across the seabed by the mooring chain, and when Φ reaches 90°, the change in bearing capacity tended to level off. Taiebat et al. (2005) employed numerical methods to analyze the bearing capacity of suction anchor foundations under individual axial, torsional, and lateral forces, mapping out failure envelopes for various load combinations. Their findings indicated that torsional loads could reduce the active earth pressure the foundation needs to withstand, significantly decreasing its ultimate axial and lateral bearing capacity.

Currently, research on marine mooring foundations including suction anchors has predominantly focused on in-plane loading, utilizing a multitude of experimental (Lu et al. 2026; Du et al. 2023; Wang et al. 2019), theoretical (Wang et al. 2024; Lin et al. 2024; Zhang et al. 2024; Cui et al. 2021; Meng et al. 2020;), and numerical studies (Li et al. 2024; Xu et al. 2024; Sujawat & Kumar 2023). However, there is a lack of research on out-of-plane loading using centrifuge experiments which can restore the stress level at the actual seabed depth, leading to a deficiency in relevant experimental data for practical engineering applications. Therefore, further experimental investigation is required to develop a more comprehensive understanding of the behavior of suction anchors under out-of-plane loading.

Based on the above analysis, this study selected an optimal loading location at $2L/3$ with a horizontal angle $\theta_m = 35°$, and a range of out-of-plane angles were established. Centrifuge model tests under 50g conditions were performed in soft clay using displacement control. Through real-time monitoring of anchor displacement, soil pressure cells, and pore pressure cells, the mechanism of bearing capacity characteristics of suction piles under out-of-plane loading was analyzed.

2 CENTRIFUGE MODELING TESTS

The model tests were carried out using the ZJU400 beam-type centrifuge at Zhejiang University, with a maximum capacity of 400 g·t, as depicted in Figure 1. The tests were performed under an acceleration of 50g. The scaling laws employed in this test were based on those proposed by Taylor (2018). Taking into account the boundary effects and the influence of the metal model box on the magnetometer, a model box with dimensions of 1.2 m × 0.95 m × 1.0 m was chosen for this test.

Figure 1. The beam centrifuge ZJU400 at Zhejiang University.

2.1 *Model anchor*

As illustrated in Figure 2, the model anchor comprises a seamless steel hollow cylinder, a POM plastic anchor cap, and

two semicircular clamps. The model anchor features a length (L_a) of 318 mm, an outer diameter (D) of 110 mm, an inner diameter (d) of 108 mm, a wall thickness (r_1) of 1 mm, a top thickness (r_2) of 10 mm, a weight (W) of 1.04 kg, and a penetration depth (L) of 300 mm, with a geometric scale ratio of 1:50 between the model and the prototype.

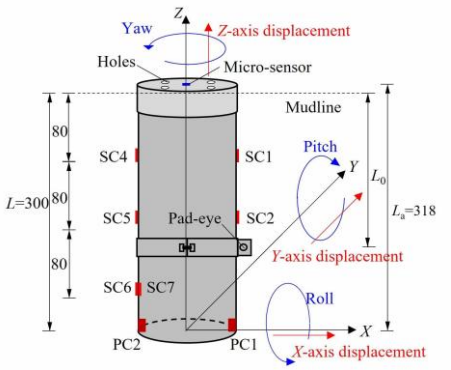

Figure 2. Model anchor and transducers arrangement (unit: mm).

2.2 *Model test foundation preparation and T-bar tests*

The study employed Malaysian kaolin clay to create a saturated soft clay foundation, The liquid limit and plastic limit of the clay were 60.7% and 36.5%, respectively, and the specific gravity was 2.60.

Dry clay powder and deionized water were blended in a mixer, while continuously applying vacuum degassing to create a saturated slurry at twice the liquid limit (w=121.4%). Following 24 hours of consolidation under 50g, the total height of the prepared model foundation and the sand cushion layer was 650 mm. T-bar tests were performed on the model seabed after each consolidation. The T-bar probe was developed by the Centre for Offshore Foundation Systems (COFS) at the University of Western Australia (White et al. 2010). The resulting undrained shear strength profile is shown in Figure 3.

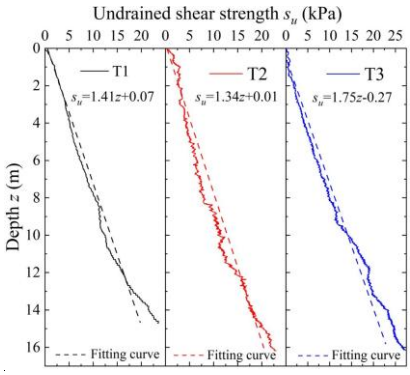

Figure 3. Undrained shear strength profile.

2.3 *Test setup*

The loading procedure is presented in Table 1. The setup for the centrifuge tests conducted on saturated soft clay is illustrated in Figure 4 (T1, Φ= 0°). The loading rate of the motor used in this study is v = 1.5 mm/s, which is greater than v_u = 90 c_v /D to meet the undrained loading rate requirement (Chen & Randolph 2007).

Table 1. Test loading program.

Test group	θ_m (°)	L_0 (mm)	Φ (°)	v (mm/s)
T1	35	2L/3	0	1.5
T2	35	2L/3	30	1.5
T3	35	2L/3	90	1.5

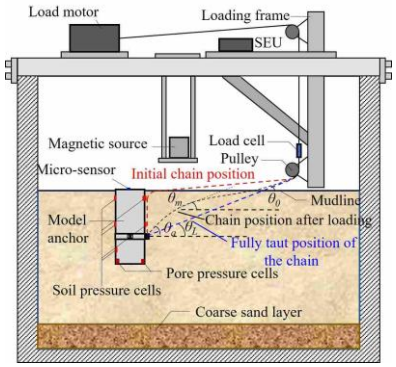

Figure 4. Test setup of model tests.

The sensors employed in this study include magnetometers, force sensors, pore pressure cells, and soil pressure cells. The Micro-Sensor 1.8TM magnetometer is capable of monitoring the displacement of the model anchor across six degrees of freedom: X-, Y-, Z-axis displacements, and rotations about X-, Y-, Z-axes (roll, pitch, yaw). The miniature sensor of the magnetometer device was positioned atop the model anchor.

After the first consolidation, a pile driver was employed to drive the model anchor vertically and at a constant speed into the test model foundation. Referencing methods used in actual engineering to mitigate soil disturbance, a second consolidation was performed for 3.5 hours under 50g. Until the pore pressure readings at the end of the model anchor stabilized, the loading test commenced and continued until the anchor body reached its ultimate bearing capacity and failed.

3 RESULTS AND DISCUSSION

3.1 *Ultimate bearing capacity*

It is crucial to regulate the bearing capacity of anchors using accurate undrained shear strength. For heterogenous soil profiles exhibiting a linear variation of undrained shear strength with depth, the method proposed by Davis and Booker (1973) was employed to calculate the equivalent undrained shear strength, thereby normalizing the measured bearing capacity. The equivalent average undrained shear strength $s_{u,avg}$ and the end resistance factor N_c for test groups T1 to T3 are calculated, as presented in Table 2.

Table 2. Ultimate bearing capacity.

Test group	$s_{u,avg}$ (kPa)	N_c	$F_{max}/s_{u,avg}A_p$	s	$F_{0.3}/s_{u,avg}A_p$
T1	10.31	9.20	8.70	0.26D	8.65
T2	9.24	8.14	7.68	0.32D	7.66
T3	10.90	7.44	7.02	0.54D	3.44

Figure 5 shows the load-displacement curve, normalized using the previously mentioned $s_{u,avg}$. According to DNV-RP-E303 (2005), the displacement range from the onset of damage to the anchorage foundation until failure is between 0.1D and 0.3D. These end values correspond to the bearing capacities $F_{0.1}$ and $F_{0.3}$, respectively. For T1 and T2, the model anchors reached their ultimate bearing capacity at approximately 0.3D. However, for T3, when the total displacement reached 0.3D, its bearing capacity was only half of the ultimate bearing capacity. This indicates that a large out-of-plane angle Φ results in a stage during the loading process where displacement increases without a corresponding increase in bearing capacity. The displacement characteristic of this stage was vertical pullout accompanied by severe twisting. When the anchor body twisted to a certain angle, the bearing capacity began to rise again. The

value of its ultimate bearing capacity is nearly equal to that of T2 under the same total displacement.

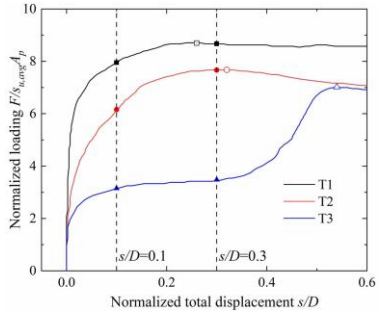

Figure 5. Variation of bearing capacity during loading with total displacement.

In selecting the bearing performance (F_p) of the anchor: If the maximum value is reached before the total displacement of the anchor body reaches 0.3D, use the corresponding ultimate bearing capacity. Otherwise, use the capacity corresponding to a total displacement of 0.3D. Figure 6 is modified from Ward et al. (2008). The vertical axis represents F_{Tn}/F_{T1}, while the horizontal coordinate represents the angle θ (rotation around the Z-axis during loading) corresponding to the capacity reaching F_p. The figure shows that the results of this test are in good agreement with the curve obtained by equilibrium analysis.

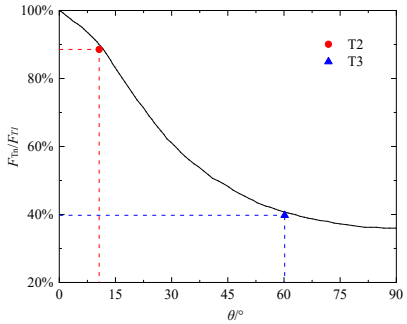

Figure 6. Effect of out-of-plane loading on suction anchor capacity.

3.2 *Failure mode*

Figure 7 illustrates the failure modes for three test groups. The failure mode of T1 is primarily translational. During loading of T2, numerous cracks emerged in the passive zone, whereas the active zone remained intact. The anchor's failure mode is primarily backward inclination. During loading of T3, the model anchor underwent considerable torsion. Circular cracks emerged on the nearby foundation surface. Neither the active nor passive zones developed any cracks. The anchor's failure mode is primarily torsional and backward inclination.

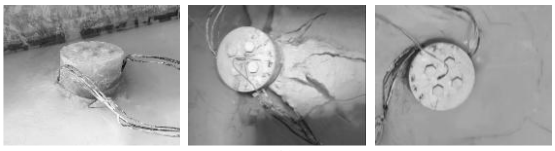

(a) (b) (c)

Figure 7. Anchor failure mode: (a). T1 translation; (b). T2 backward rotation; (c). T3 torsion and backward rotation.

The above analysis shows that the two test groups, T2 and T3, exhibit significantly different twisting time and failure modes during loading. Figure 8 illustrates the variation curve of the twisting angle θ around the Z-axis with the total displacement during loading. It was evident that for test T2 (Φ=30°), θ increased almost linearly with displacement throughout the entire loading process. For test T3 (Φ = 90°), the anchor body underwent more violent twisting between a total displacement of 0.1D and 0.3D. As shown in Figure 5, the bearing capacity of the anchor remained almost unchanged during this period, with the displacement primarily being vertical. When the difference between Φ and θ approached 30°, its rate of angle change was identical to T2. For in-plane loading, the resistance of the soil to the anchor is mainly provided by the friction at the anchor-soil interface and the bearing resistance of the soil at the anchor tip. As the applied load surpasses the ultimate bearing capacity of the anchor, shear failure is induced in the surrounding soil mass, leading to horizontal displacement of the anchor. Meanwhile, an increase in the out-of-plane loading angle results in a corresponding increase in the torque acting on the anchor. Once the torque reaches a critical value, the anchor initiates a twisting motion, which in turn induces rotational movement in the adjacent soil.

Thus, the torsion resulting from a large out-of-plane angle Φ does not grow linearly with the overall displacement, instead, it comprises two phases. Phase 1: The anchor experiences substantial rotation along with some displacement, and following this rotation, the anchor's bearing capacity ceases to increase notably. Phase 2: The load on the anchor transitions from a large out-of-plane angle Φ to a small one, altering the failure mode. During this phase, the anchor's bearing capacity rises again, with its ultimate bearing capacity being similar to that under a small out-of-plane angle Φ for the same overall displacement. The demarcation point between these two phases is determined by the value of (Φ-θ). In this experiment, this value appears to be approximately 30°, although there are factors affecting this threshold, such as the geometric dimensions of the suction anchor, soil conditions and loading rate. Therefore, further experimentation is required to confirm this value. Nevertheless, the two-phase failure pattern for large out-of-plane angles Φ is clearly discernible in this experiment. Therefore, based on these differing failure modes, an out-of-plane load angle $\Phi < 30°$ is categorized as "small" out-of-plane load angle while $30° < \Phi < 90°$ is considered a "large" one.

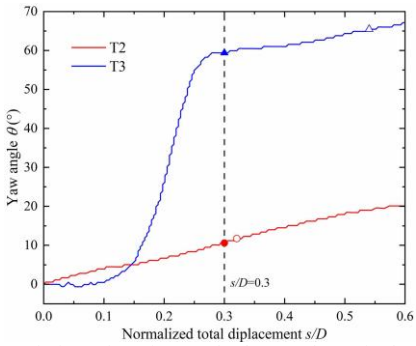

Figure 8. Variation of torsion angle θ around Z-axis during loading with total displacement.

3.3 *Response of pore pressure and soil pressure*

Figure 9 presents the soil pressure and pore pressure responses for test T2, revealing a clear distinction between active and passive zones around the anchor. The presence of the out-of-plane angle Φ transforms the failure mode from pure translation to a backward tilting motion. Thus, the upper soil pressure cell (SC 4) on the backside of the anchor showed a marked increase. SC 4's response reached its peak near the ultimate bearing capacity. SC 1 and SC2 showed little change and SC 3 exhibited a certain degree of increase. All other cells on the backside of the anchor, except for SC 4, showed a decrease. The pore pressure response peaked at s/D = 0.15. Moreover, the response of pore pressure cell (PC 2) on the backside of the anchor is

stronger than that of forward one (PC 1). The ultimate bearing capacity corresponds to an *s/D* value of 0.32.

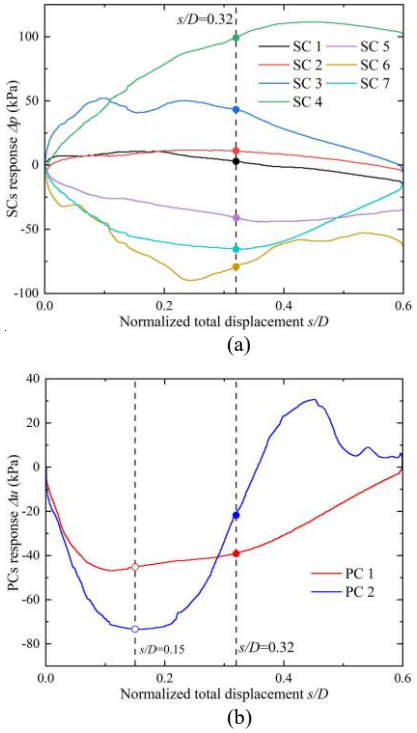

Figure 9. T2: (a) soil pressure cells response; (b) pore pressure cells response.

Figure 10 presents the soil pressure and pore pressure responses observed in test T3. During the initial stage of anchor displacement, characterized by severe torsion without a significant increase in bearing capacity, none of the soil pressure cells exhibited a strong response. The pore pressure cells registered some response, thereby ensuring a certain level of bearing capacity during the first stage. As the second stage commenced, marked by a decrease in torsion and a renewed increase in bearing capacity, the soil pressure cells gradually exhibited a more substantial response, however, this response exhibited a certain degree of delay. Owing to the backward inclination of the anchor body, soil pressure cell 4 (SC 4) continued to show a significant increase. The response of soil pressure cell 4 reached its peak near the ultimate bearing capacity. In contrast, the response of the soil pressure cell on the front side of the anchor was weaker compared to T2. The pore pressure response was more pronounced compared to the first stage. Furthermore, the displacement corresponding to the ultimate bearing capacity remained greater than the displacement associated with the peak pore pressure.

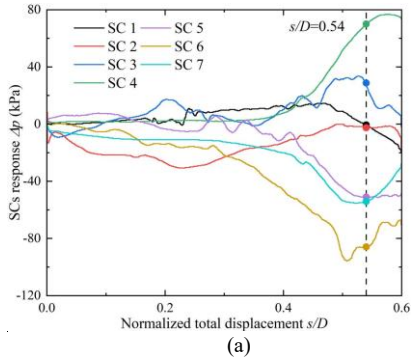

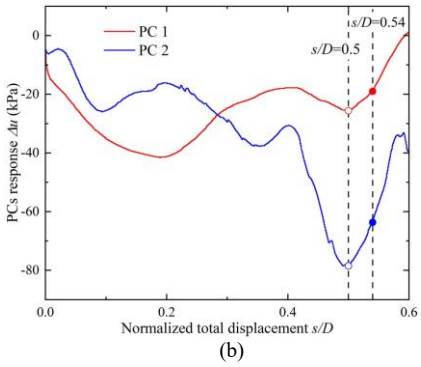

Figure 10. T3: (a) soil pressure cells response; (b) pore pressure cells response.

4 LIMIT EQUILIBRIUM METHOD

4.1 *Weakening in bearing capacity under small out-of-plane loading angles*

Because of the large aspect ratio of the suction anchor, its failure mode is generally dominated by vertical pullout. Generally, its vertical bearing capacity reaches the limit value before the lateral does. Moreover, as clearly seen in section 3.3, the out-of-plane load angle has minimal impact on the horizontal failure mode of the anchor. Therefore, the discussion of bearing capacity degradation caused by torsion from the out-of-plane load angle primarily focuses on the degradation of vertical bearing capacity. Subsequently, the corresponding weakened lateral bearing capacity is calculated based on the motion direction angle β. In the case of overall failure, the vertical pullout resistance of the suction anchor (2002) is:

$$P_u = F_{ext} + R_u = \alpha s_{u,avg} A_s + \zeta_{ce}\zeta_{cs} N_c s_{u,avg} A \qquad (1)$$

where α is the friction coefficient; A_s is the friction area of the anchor's outer wall, its value is πDL; A is the base area of the anchor end, its value is πR^2; ζ_{ce} and ζ_{cs} are coefficients considering the foundation embedding and shape, with the value of 1.49 and 1.2, respectively. By applying the above formula, the vertical bearing capacity is determined to be 1.83 kN under conditions of the in-plane condition. By utilizing the loading inclination angle θ_a at the pad-eye, the corresponding inclined bearing capacity is computed as 3.06 kN, which is close to the measured value of 3.12 kN from the centrifugal test.

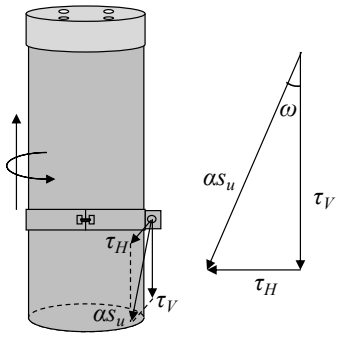

Figure 11. Schematic diagram of the effect of torsion on anchor bearing capacity.

In test T2, where the out-of-plane load angle is relatively small, the failure zones induced by the anchor's end bearing capacity and the soil resistance at the base scarcely overlap with the failure surface caused by torque (Taiebat et al. 2005), therefore, the impact of torsion on the anchor's end bearing capacity is neglected. The primary mechanism by which torsion weakens the anchor's bearing capacity is that the torque causes

the soil's shear strength to no longer simply resist vertical forces, but instead generates a horizontal shear resistance component (as illustrated in Figure 11), at this time, there is:

$$(\alpha s_u)^2 = \tau_V^2 + \tau_H^2 \quad (2)$$

where τ_V is is the vertical shear force of soil; τ_H is the horizontal shear force of soil; that is, the first term in Equation (1), where torsion induces a lateral shear force, necessitating a corresponding horizontal shear resistance component from the soil, thereby weakening the anchor's vertical bearing capacity, resulting in a weakened vertical uplift resistance of:

$$P_u = \alpha s_{u,avg} A_s \cos\omega + \zeta_{ce}\zeta_{cs} N_c s_{u,avg} A \quad (3)$$

where ω is the angle between the vertical shear resistance component and the shear resistance of the soil, which can be obtained from the torque T generated by the horizontal shear resistance component of the soil:

$$\omega = \sin^{-1}\frac{T}{2\alpha s_{u,avg} A_s R} \quad (4)$$

By utilizing the loading angle θ_a and bearing capacity F obtained from the centrifuge test for T2, the vertical component of the bearing capacity was calculated as $P_u = F\sin\theta_a$, which equals 1.40 kN. Substituting this value into Equation (4), the value of ω equaled 50.5°. This indicates that for the reduction in bearing capacity caused by torsion due to the small OOP load angle, the primary factor to consider is the attenuation of the lateral frictional force, F_{ext}. The weakening coefficient, represented by $\cos\omega$, was calculated to be 0.636 in this test.

As shown in Figure 8 of section 3.2, T2 (Φ = 30°) experienced a uniform torsional rate during the entire loading process, without any abrupt changes in the torsion angle, and T3 also ceased severe torsion when the OOP load angle reached about 30° in the out-of-plane load direction. Therefore, excluding the impact of extreme environmental loads, and under undrained loading conditions, at a lower loading rate, Φ = 30° can be considered as the threshold value for the OOP load angle in this test. When addressing small OOP load angles (Φ < 30°), a reduction factor of 0.636 can be applied to account for the decrease in bearing capacity due to torsion.

4.2 *Analysis of bearing capacity under large out-of-plane loading angles*

In test T3, where the OOP load angle was relatively large, a significant torque developed as the external load increased, causing the anchor to twist violently, ultimately leading to failure. At this point, the external load remained relatively small and the vertical component of it could be neglected, and the vertical shear component of the soil was assumed to be zero, meaning the shear strength of the soil outside the anchor was considered in relation to the horizontal force:

$$T_1 = \frac{D}{2}\int_0^L \pi D\tau_H dz = \frac{\pi D^2 L}{2}\alpha s_{u,avg} \quad (5)$$

In cases where the failure mode is torsional, beyond the previously mentioned torsional resistance T1 offered by the soil, there exist two further potential torsional resistances: If the soil plug inside the anchor does not twist together with the anchor body, the inner wall of the anchor will exhibit a torsional resistance equivalent to that of the outer wall. If the soil plug inside the anchor twists along with the anchor body, a torsional resistance will be generated at the anchor end, and its calculation formula is as follows:

$$T_2 = \int_0^R 2\pi r^2 s_{u,bot} dr = \frac{2\pi R^3}{3} s_{u,bot} = \frac{\pi R^3}{12} s_{u,bot} \quad (6)$$

where $s_{u,bot}$ is the undrained shear strength at the anchor's end. Upon the anchor body experiencing distinct torsional failure, the failure can be categorized into two modes depending on whether the soil plug within the anchor rotates along with it. The respective calculation formulas are as follows:

$$T = \pi D^2 L\alpha s_{u,avg} \quad (7)$$

$$T = \frac{\pi D^2}{2}\left(\alpha L s_{u,avg} + \frac{D}{6} s_{u,bot}\right) \quad (8)$$

Equation (7) represents the first failure mode, in which the soil plug within the anchor remains stationary as the anchor body rotates. Equation (8) indicates the second failure mode, characterized by the soil plug inside the anchor rotating in unison with the anchor body. In typical scenarios involving a substantial OOP load angle (resulting in pronounced torsional failure), the lesser of the two torsional resistances should be considered the ultimate torsional resistance, namely when:

$$\frac{\pi D^2 L}{2}\alpha s_{u,avg} < \frac{\pi R^3}{12} s_{u,bot} \quad (9)$$

where $s_{u,bot}$ is the undrained shear strength at the anchor's end, $s_{u,avg}$ is the equivalent average undrained shear strength, and the ratio between them is roughly 2. If the conditions of the aforementioned equation are satisfied, the anchor experiences the first mode of failure, conversely, the second type of failure takes place. By simplifying the above expression, we get:

$$T = \pi D^2 L\alpha s_{u,avg} \quad \left(\frac{L}{D} < \frac{1}{3\alpha}\right) \quad (10)$$

$$T = \frac{\pi D^2}{2}\left(\alpha L s_{u,avg} + \frac{D}{6} s_{u,bot}\right) \quad \left(\frac{L}{D} > \frac{1}{3\alpha}\right) \quad (11)$$

As observed in Figure 8 of section 3.2, during T3, from the initiation of significant torsional rotation of the anchor to an angular rotation of θ = 60° around the Z-axis, the torsional resistance offered by the soil was substantially lower than the external torsional force induced by Φ. Upon reaching θ = 60° (where the out-of-plane load angle became Φ - θ = 90° - 60° = 30°, identical to the initial out-of-plane load angle in T2), the anchor ceased to experience significant torsional rotation. At this point, the total displacement s of the anchor body also reached approximately 0.3D. It can be inferred that as the anchor rotated towards the direction of the out-of-plane load, T correspondingly decreased. When it diminished to a level equal to the torsional resistance provided by the soil, the intense torsional rotation ceased. At this juncture, it can be regarded that the ultimate torsional resistance the soil can offer equals the torque induced by the external force at two distinct moments. The first moment occurs at Φ = 90°, where the anchor reached a critical state on the verge of torsional rotation. Since at this Φ angle, minute displacement variations can result in substantial changes in external force, accurately determining the magnitude of the external load became challenging. Consequently, the second moment was employed to calculate the ultimate torsional resistance, corresponding to the external force and out-of-plane load angle when the anchor ceased intense torsional rotation (at this point, Φ = 30°, with the direction of motion angle being β). Furthermore, in T2 (Φ = 30°), it was also observed that the failure mode involved the anchor undergoing gradual torsional failure, which permeated the entire loading process. Therefore, it can be concluded that at Φ = 30°, the torsional resistance generated by the horizontal shear resistance of the soil equated to the torque produced by the external load:

$$T = FR\cos\beta\sin 30^\circ = \frac{FR\cos\beta}{2} \quad (12)$$

Solving Equations (10) to (12) yields the ultimate bearing capacity of the anchor under torsional failure mode:

$$F = \frac{4\pi D^2 L \alpha s_{u,avg}}{\cos\beta} \quad (\frac{L}{D} < \frac{1}{3\alpha}) \tag{13}$$

$$F = \frac{2\pi D}{\cos\beta}\left(\alpha L + \frac{D}{3}\right) s_{u,avg} \quad (\frac{L}{D} > \frac{1}{3\alpha}) \tag{14}$$

Using the length-diameter ratio and friction coefficient of the model anchor from the experiment, and substituting the relevant T3 data into Equation (14), the limit equilibrium analysis method yielded an F value of 1.07 kN, which is less than the 1.31 kN measured in the centrifuge test. This discrepancy might stem from neglecting the vertical component of the external load, assuming a zero vertical shear component in the soil. However, in practical engineering, the soil's vertical shear component cannot be zero and still adheres to the relationship in Equation (2). This leads to an underestimation of F, but it is conservatively safe for engineering, because there was more safety margin during the design process. Thus, the calculated ultimate bearing capacity of the suction anchor at torsional failure, using this method, is relatively reasonable.

5 CONCLUSIONS

This paper conducts a series of centrifuge model tests on the out-of-plane inclined loading of the suction anchor to deeply explore the influence of the out-of-plane load angle Φ on the bearing capacity and failure mode of the anchor, and carries out limit equilibrium analysis, drawing the following conclusions.

1. Based on centrifuge tests and limit equilibrium analysis, a critical OOP load angle threshold of 30° is established as a key design criterion.
2. For small angles ($\Phi < 30°$), a recommended weakening coefficient of 0.636 should be applied to the side friction term in bearing capacity calculations to account for torsional effects, leading to an approximate 12% capacity reduction.
3. For large angles ($30° < \Phi < 90°$), the failure mode shifts to a complex torsional-rotational mechanism. Design must then use the proposed limit equilibrium method (Equations (13) and (14)), which is governed by the anchor's aspect ratio (L/D) and friction coefficient (α).

6 ACKNOWLEDGEMENTS

The fundings supported by the National Natural Science Foundation of China (No. 52279112 and No. U23A20670) and Natural Science Foundation of Jiangsu Province (BK20241057) are gratefully acknowledged.

7 REFERENCES

Aubeny, C. 2017. *Geomechanics of marine anchors*. Florida: CRC Press, 27-28.

Cui, C., Meng, K., Xu, C., Liang, Z., Li, H. and Pei, H. 2021. Analytical solution for longitudinal vibration of a floating pile in saturated porous media based on a fictitious saturated soil pile model. *Computers and Geotechnics*, 131, 103942.

Chen, W., Randolph, M.F. 2007. Uplift capacity of suction caissons under sustained and cyclic loading in soft clay. *Journal of Geotechnical and Geoenvironmental Engineering*, 133(11): 1352-1363.

Chen, W., and Randolph, M.F. 2007. External radial stress changes and axial capacity for suction caissons in soft clay. *Géotechnique* 57(6): 499-511.

Colliat, J.L., Safinus, S., Boylan, N., Schroeder, K. 2018. Formation and development of seabed trenching from subsea inspection data of deepwater Gulf of Guinea moorings. *Offshore Technology Conference*, OTC, Houston, OTC-29034-MS.

Davis, E.H., and Booker, J.R. 1973. The effect of increasing strength with depth on the bearing capacity of clays. *Géotechnique* 23(4): 551-563.

Lu, W., Cai, D., Li, J. and Wang, A. 2026. The Role of Shared Suction Anchors for Mitigating Cascading Failure in Floating Offshore Wind Farms. *Computers and Geotechnics*, 189, 107655.Du, S., Wang, C., Zhang, Z., Wu, G., Liang, B., 2023. Experimental Study of Local Scour Around Circularcrossing and Square-Crossing Piles in Waves and Current. *Journal of Marine Environmental Engineering*. 11(1).

Li, J., Cui, C., Xiao, Z., Wang, B. and Xu, C. 2024. Reliability and sensitivity analyses of monopile supported offshore wind turbines based on probability density evolution method with pre-screening of controlling parameters. *Ocean Engineering*, 310, 118746.

Liu, H., Nagula, S., Jostad, H.P., Piciullo, L. and Nadim, F. 2024. Considerations for using critical state soil mechanics based constitutive models for capturing static liquefaction failure of tailings dams. *Computers and Geotechnics*, 167, 106089.

Lin, J., Zhang, L., Liao, C., Zhang, J., Yang, H., Zhang, Z. and Wang, W. 2024. Probabilistic calibration of the p-y method considering model uncertainty for ultimate limit state design of monopiles. *Georisk: Assessment and Management of Risk for Engineered Systems and Geohazards*, 18(3): 687-705.

Meng, K., Cui, C., Liang, Z., Li, H. and Pei, H. 2020. A new approach for longitudinal vibration of a large-diameter floating pipe pile in visco-elastic soil considering the three-dimensional wave effects. *Computers and Geotechnics*, 128, 103840.

Sujawat, R.S. and Kumar, R. 2024. Stochastic numerical analyses to investigate the effects of the spatial nonuniformity of offshore ground on the serviceability of monopile foundations. *Georisk: Assessment and Management of Risk for Engineered Systems and Geohazards*, 18(3): 591-608.

Taiebat, H.A., and Carter, J.P. 2005. A failure surface for caisson foundations in undrained soils. *Proc. 1st International Symposium on Frontiers in Offshore Geotechnics*, Perth, 289-295.

Taylor, R.N. 2018. *Geotechnical Centrifuge Technology*. London: Taylor & Francis.

Veritas, D.N., 2005. Geotechnical design and installation of suction anchors in clay. *DNV Recommended Practice RP-E303*. Høvik.

Ward, E.G., Mercier, R.S., Zhang, J., Kim, M.H., Aubeny, C., Gilbert, R.B. 2008. Final Project Report Prepared for the Minerals Management Service Under the MMS/OTRC Cooperative Research Agreement. *Offshore Technology Research Center*, Texas.

Wang, B., Cui, C., Xu, C., Meng, K., Li, J. and Xu, L. 2024. A novel analytical solution for horizontal vibration of partially embedded offshore piles considering the distribution effect of wave loads. *Ocean Engineering*, 307, 118179.

Wang, H., Su, L., Zhang, M.S., Liu, H.J., 2020. Effects of Storm Wave-Induced Liquefaction On Lateral Deformation of Monopile-Type Offshore Wind Turbines in Silt Seabed. *Journal of Marine Environmental Engineering*, 10(3): 225-242.

Wu, M., Zhao, Z., Rong, Q., Cai, G., Duan, W. and Wang, C. 2024. Evaluating undrained shear-strength of marine clay using free-fall penetration considering uncertainty: an experimental and Bayesian analysis study. *Georisk: Assessment and Management of Risk for Engineered Systems and Geohazards*, 18(3):706-726.

White, D.J., Gaudin, C., Boylan, N. Zhou, H. 2010. Interpretation of T-bar penetrometer tests at shallow embedment and in very soft soils. *Canadian Geotechnical Journal*, 47(2): 218-229.

Xu, S.J., Yi, J.T., Yi, J.W., Li, X.B., Tian, Y., Xie, Q. and Liu, F. 2024. Effects of random heterogeneity of soil on VH failure envelopes of the torpedo anchor. *Georisk: Assessment and Management of Risk for Engineered Systems and Geohazards*, 18(2): 447-466.

Yan, L., Yang, J., Wu, Y., 2024. Shear Strength of Yellow River Estuary Soil Solidified by Using All-Solid-Waste Binder in Protecting Foundations of Offshore Wind Turbines. *Journal of Marine Environmental Engineering*, 11(4).

Zhang, Y., Huang, J., Xie, J., Giacomini, A. and Zeng, C. 2024. Updating reliability of pile groups with load tests considering spatially variable soils. *Georisk: Assessment and Management of Risk for Engineered Systems and Geohazards*, 18(4): 750-764.

Sun, L., Zhang, Y., Feng, X., Gourvenec, S. and Li, S. 2024. Upper-bound solutions for inclined capacity of suction caissons in a trenched seabed. *Géotechnique* 74(5), 473-485.